

RESEARCH

Open Access



Tensile Fracture Property of Concrete Affected by Interfacial Transition Zone

Heli Ji², Xinhua Yang^{1,2*}, Zuyun Luo² and Fan Bai³

Abstract

As a weak link between aggregate and mortar in concrete, interfacial transition zone (ITZ) usually plays a key role in concrete fracture. To investigate the tensile fracture property of concrete affected by the mechanical properties of ITZ numerically, the geometrical models of heterogeneous concrete were established with the parameterization modeling. They include three phases, namely, mortar, ITZ, and randomly distributed aggregates with distinct sizes and orientations. The cracking behaviors of mortar and ITZ were characterized by the bilinear cohesive zone constitutive model. Based on the experiments, the mechanical properties of ITZ were mediated by changing the water–cement ratio of mortar, the aggregate surface roughness and the content of silica fume in interfacial agent. A series of numerical simulations were conducted on the concrete models in tension after the numerical modeling method was validated. The macroscopic tensile fracture properties of concrete were quantitatively connected with some microscopic variables, including the water–cement ratio of mortar, the aggregate surface roughness and the silica fume content in interfacial agent. It was found that the tensile fracture properties of concrete have negative linear correlations with the water–cement ratio of mortar, while the effects of the aggregate surface roughness and the silica fume content in interfacial agent are very complex. The tensile fracture mechanical properties of concrete have a bilinear relationship with the aggregate surface roughness and an approximate quadratic parabola relationship with the content of silica fume in the interfacial agent. This study is beneficial to improve the fracture resistance of concrete by some interface handling measures.

Keywords: Concrete, Interfacial transition zone, Parameterization modeling, Fracture property

1 Introduction

As the most widely used engineering building material, concrete has many advantages, including low price, easy construction, mechanized mass production, high compressive strength, good durability and wide strength grade. Concrete consists of aggregate, mortar and their interfacial transition zone (ITZ). Compared with mortar matrix, the ITZ usually has larger porosity (Liao et al., 2004; Tschegg et al., 1995; Yang, 1998), higher water–cement ratio and permeability (Scrivener et al., 2004),

and lower strength, toughness (Wu et al., 2016) and elastic modulus (Bourdette et al., 1995), so it is a weak link between aggregate and mortar in concrete and cracks tend to occur and propagate inside it. Accordingly, the ITZ property generally has a great influence on the fracture property of concrete, and to a certain extent determines crack path selection, as well as adhesion or cohesion failure mode of concrete subjected to external loads (Chen & Qian, 2017; Ding & Chen, 2019; Hong et al., 2014; Zhang et al., 2018a, 2018b).

In general, there are two internal mechanisms for the bonding between aggregate and mortar (Guinea et al., 2002; Liao et al., 2004). One is the physical bonding mechanism. The bonding force is mainly related to the mechanical interlocking between the aggregates and the mortar matrix, and depends on the mineral properties

Journal information: ISSN 1976-0485/eISSN 2234-1315.

*Correspondence: yangxinh@hust.edu.cn

¹ School of Transportation, Civil Engineering and Architecture, Foshan University, Foshan 528200, China

Full list of author information is available at the end of the article



© The Author(s) 2022. **Open Access** This article is licensed under a Creative Commons Attribution 4.0 International License, which permits use, sharing, adaptation, distribution and reproduction in any medium or format, as long as you give appropriate credit to the original author(s) and the source, provide a link to the Creative Commons licence, and indicate if changes were made. The images or other third party material in this article are included in the article's Creative Commons licence, unless indicated otherwise in a credit line to the material. If material is not included in the article's Creative Commons licence and your intended use is not permitted by statutory regulation or exceeds the permitted use, you will need to obtain permission directly from the copyright holder. To view a copy of this licence, visit <http://creativecommons.org/licenses/by/4.0/>.

and surface texture characteristics of aggregates (Caliskan, 2003; Gu et al., 2013; Hong et al., 2014; Rao & Prasad, 2004; Shen et al., 2019), as well as their shape and size (Caliskan, 2003). The other is the chemical bonding mechanism. When the aggregates are chemically active to the mortar, a chemical bond would be formed between the two (Asbridge et al., 2001; Bui et al., 2005; Duan et al., 2013; Ji et al., 2020; Jiang, 1999; Kuroda et al., 2000; Rossignolo, 2009; Siddique, 2011). Thus, the properties of ITZ can be physically or chemically changed. For example, it is believed that there is a poor bonding between the cement paste and asphalt-coated aggregates. Brand and Roesler () compared the ITZ for mortar with reclaimed asphalt pavement (RAP) aggregates relative to dolomite aggregates through image analysis of back-scattered electron micrographs. They found that the ITZ with RAP aggregates was larger and more porous with less calcium silicate hydrate and calcium hydroxide at the interface than the ITZ with dolomite aggregates.

Based on the abovementioned two mechanisms of interfacial interaction, the ITZ properties can be improved from the following three aspects: (a) selecting appropriate aggregate type and aggregate size combination, and improving aggregate surface roughness (Caliskan, 2003; Jiang, 1999; Rao & Prasad, 2004; Shen et al., 2019); (b) adding mineral additives or admixtures with good compactness and chemical activity into the mortar (Asbridge et al., 2001; Duan et al., 2013; Jiang, 1999; Rao & Prasad, 2004); and (c) treating the aggregate surface chemically to produce functional groups that can be coupled to the mortar. Among them, the use of mineral additives or admixtures is a very effective way to improve the ITZ properties. For example, fly ash and silica fume were, respectively, added to concrete as the substitutes for cement to improve the mechanical properties of concrete (Golewski, 2021a, 2021b, 2021c; Szostak & Golewski, 2020). It was demonstrated by a variety of experimental means that these additives could significantly increase the strength and fracture toughness of concrete and reduce the micro-crack size in the ITZ of concrete. The effects of fly ash and silica fume on the fracture properties of high-performance concrete were also experimentally investigated (Smarzewski, 2019; Zhang & Li, 2012). In these studies, however, the additives were added to cement paste, so that they affect not only the interface properties but also the properties of the matrix material.

By improving the adhesive effect of ITZ, the mechanical properties of concrete can be enhanced effectively. Due to the complex internal structure of concrete, different shapes and sizes of aggregates, and their random distribution, there are many factors affecting the ITZ bonding effect. Accordingly, it is very difficult to evaluate quantitatively the contribution of the ITZ property

improvement to the macroscopic mechanical properties of concrete based on experiments, excluding the mortar property effect.

Many efforts have been made to develop numerical micromechanical models capable of predicting the mechanical behavior of heterogeneous concrete. For example, a concurrent multiscale modeling approach was proposed by Rodrigues et al. (2021; Rodriguesa et al., 2020) to investigate crack propagation in conventional concrete and recycled aggregate concrete. Utilizing the “take-and-place” method, coarse aggregates with regular shapes were generated from a given grading curve and then placed into the mortar matrix randomly. The mesh fragmentation technique (Manzoli et al., 2016; Sánchez et al., 2014) was used to treat the cracking of mortar and ITZ by introducing interface solid finite elements equipped with a tensile damage model. Recently, a modeling procedure named “mesh-placement-identification-assignment” was developed by Zheng et al. (2021) to establish the mesoscale concrete model composed of aggregate and mortar. The effects of aggregate shape and aggregate content on the tensile strength of concrete were discussed. In our previous work (Yang et al., 2012; Yin et al., 2011, 2012, 2015), the parameterization modeling was also developed for heterogeneous asphalt mixture and concrete. In the parameterization modeling, polyhedral or polygonal aggregates with a certain volume content and gradation were generated through some given parameters, and then randomly packed in a specified area to establish a numerical model of concrete including aggregates, matrix and their ITZs. Accordingly, it is potential that the parameterization modeling can be combined with experiments to investigate quantitatively the effect of the ITZ property improvement to the mechanical properties of concrete.

Recently, the effects of water–cement ratio of mortar, aggregate surface roughness and the content of silica fume in interface agent on the tensile fracture properties of ITZ were studied through the three-point bending test (Ji et al., 2020) and the splitting test (Zou et al., 2021) on the granite-mortar hybrid specimens. Based on the fitted experimental curves, the ITZ properties can be mediated by changing the water–cement ratio of mortar, aggregate surface roughness and the content of silica fume in interface agent. With the help of the parameterization modeling, the tensile fracture behaviors of concrete are simulated to investigate the direct improvement of the tensile fracture property of concrete from the improved ITZ properties quantitatively in this paper. This is very beneficial for engineering applications of concrete.

2 Numerical Modeling Method and Validation

2.1 Parameterization Modeling

Taking the creation of two-dimensional concrete model as an example, the main steps of parameterization modeling (Yang et al., 2012; Yin et al., 2011, 2012, 2015) are introduced as follows.

The first step is to determine the total area of all diameter levels of aggregates according to a given aggregate gradation. The aggregate size of 4.75 mm was used as the cutoff size distinguishing coarse and fine aggregates (Li & Metcalf, 2005). The coarse aggregates are dispersed in the concrete as the reinforcing phase, while the fine aggregates are combined with cement and water to form the mortar matrix. To improve the modeling efficiency, circular aggregates would be first generated and randomly packed into a prescribed region, and then inscribed into the corresponding regular octagons, as shown in Fig. 1. In view of the loss of aggregate area caused by the inscription, it is necessary to modify the total areas of the aggregates with different particle sizes by means of the area conversion factor, $k = 2\sqrt{2}/\pi$.

The second step is to generate and pack circular aggregates. The generated circular aggregates with different sizes are randomly packed into a region, whose shape and size is prescribed according to the real specimen. To avoid conflicts between packed aggregates, their sizes are reduced by a common shrinking factor before packed, and restored to their original sizes after packed.

The third step is to perform a perturbation process until a stable equilibrium is reached for the aggregate system. After all the aggregates are restored to their initial sizes,

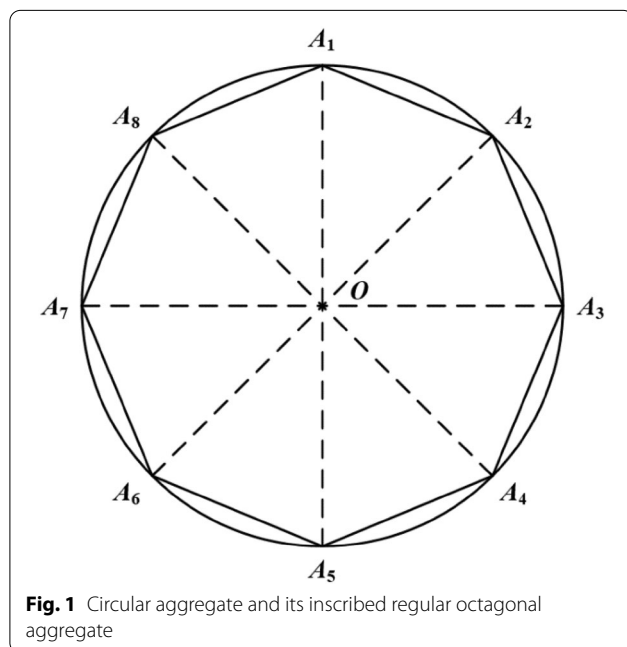


Fig. 1 Circular aggregate and its inscribed regular octagonal aggregate

a number of conflicts would inevitably occur between aggregates and aggregates or the wall, namely, the packing region boundary. It is necessary to redistribute their locations under the great repulsive forces between them through the perturbation process, so as to form a reasonable aggregate distribution.

In the fourth step, the circular aggregates are inscribed to their corresponding regular octagonal ones, so that the effect of aggregate shape can be considered in numerical simulations.

More detailed descriptions on the parameterization modeling can be seen in Ref. (Yin et al., 2012).

2.2 Cohesive Constitutive Model

It is assumed that the material is composed of simple cells connected by some virtual bonding surfaces, and damage and fracture only occur on these virtual bonding surfaces (Zhang et al., 2016). When the stress on a certain bonding surface exceeds the strength of the material, it would open (Yin et al., 2012, 2015). In general, there is a nonlinear relationship between the stress acting on the bonding surface and its relative displacement. The graphical area enclosed by the stress–displacement curve and the horizontal axis is called the fracture energy.

It is further assumed that the relationship between the stress σ and the displacement δ can be described by a bilinear model (Zhang et al., 2018a, 2018b), as shown in Fig. 2. It has two independent parameters: the bond strength t_0 and the critical displacement δ_c . When the stress is lower than the bond strength, the material is linear elastic, but after the stress reaches the bond strength, the material enters the linear softening stage and local damage occurs on the bonding surface. Finally, when the displacement reaches the critical displacement, the bonding surfaces would completely separate

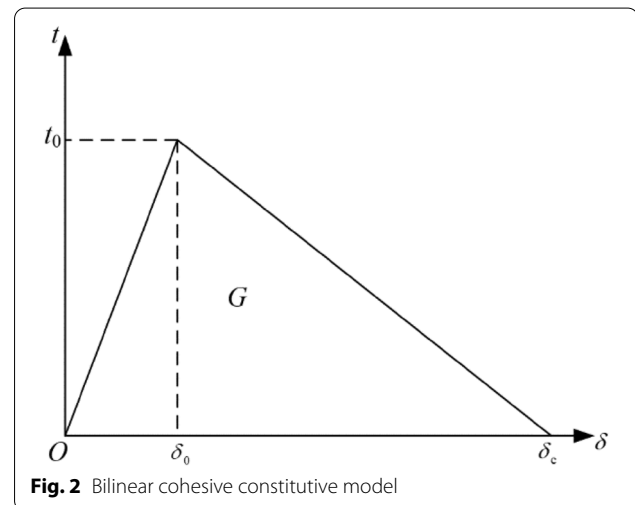


Fig. 2 Bilinear cohesive constitutive model

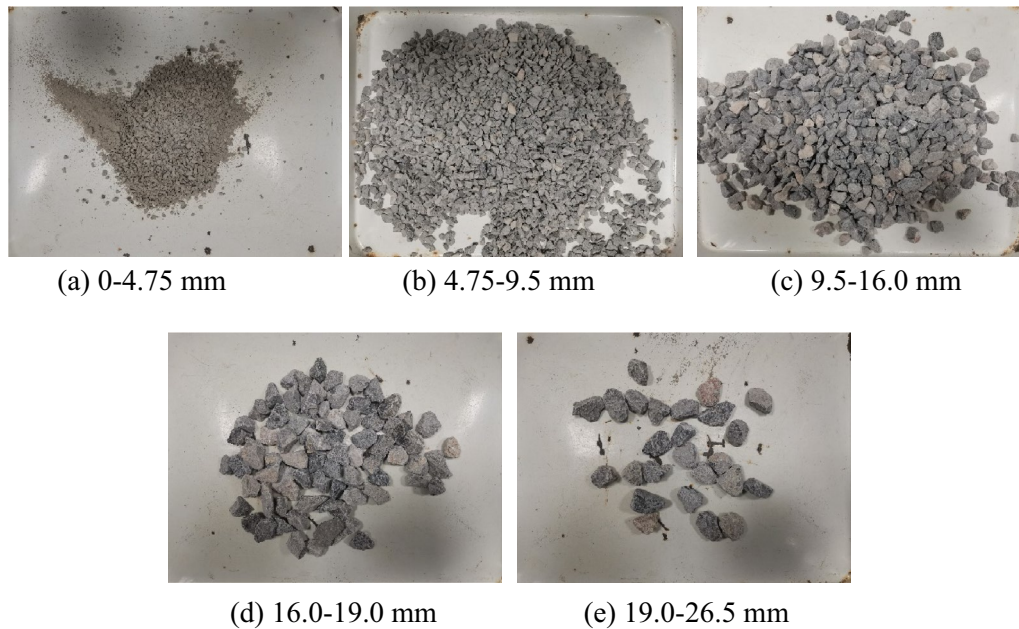


Fig. 3 Sieved fine and coarse aggregates with different diameters

Table 1 Coarse aggregate gradation

Sieve diameter (mm)	4.75	9.5	16.0	19.0	26.5
Percentage passing (%)	3.86	33.57	42.18	13.05	7.34

Table 2 Concrete mix ratio

Raw materials	Water	Cement	Fine aggregate	Coarse aggregate
Amounts (kg/m ³)	175.5	351	766.8	1106.7

and a macro-crack would start. This is the bilinear cohesive constitutive model. In this case, the fracture energy $G = 1/2\delta_c t_0$.

When simulating the fracture process of concrete, considering that aggregates usually have higher cracking resistance than mortar matrix and ITZ, it is reasonably assumed that a crack can only form and propagate in the mortar matrix and ITZ. To save computing resources, the cohesive elements with zero thickness were inserted only in the mortar matrix and ITZ in finite-element modeling. More details can be found in Ref. (Yin et al., 2012, 2015).

2.3 Three-Point Bending Fracture Experiment

To verify the feasibility of the above numerical simulation method, the three-point bending fracture experiments were carried out on six concrete specimens in the same batch. The experimental raw materials included P.I.42.5 type cement, crushed stone as coarse aggregate, medium sand as fine aggregate, and ordinary tap water, as shown in Fig. 3. After the crushed stones were screened by the sieving shaker, the 5-grade aggregates were obtained, as shown in Table 1. The concrete mix ratio is shown

in Table 2. The mass ratio between water, cement and medium sand is 1:2:4.37.

The concrete specimen size is 400 mm × 100 mm × 100 mm. After poured in the mold, the concrete was fully tamped in the vibrostand. The specimen was released from the mold after being placed in the room for 24 h, and cured in the standard curing room for 7 days. Then, a 20 mm deep notch was cut in the middle span of the length direction of the specimen with the help of a diamond saw blade under a low machining speed and water-cooling conditions.

The experiment was carried out on the WDW-100E universal testing machine. The loading setup is shown in Fig. 4, and the spacing between the two supports is 300 mm. During the experiment, the loading head slowly descends and contacts with the specimen. To fully reduce the gap between the loading head and the specimen, a load of 0.5 kN was applied in advance, followed by stable loading at a constant rate of 0.1 mm/min until the specimen was completely broken. During the loading process, the load and the displacement of the loading head were measured by the built-in sensors of the testing machine.



Fig. 4 Experimental setup of three-point bending

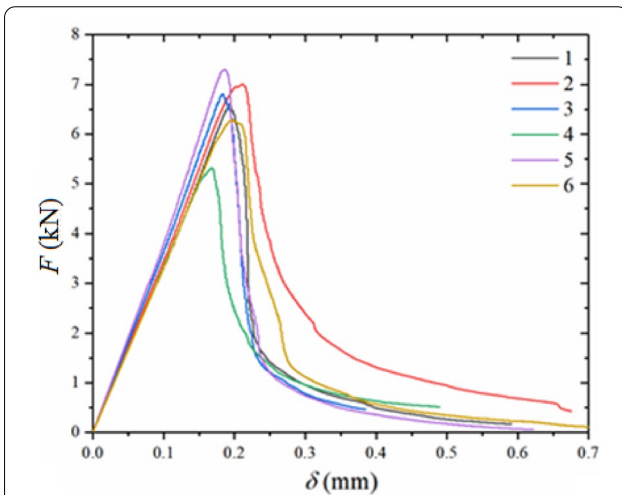


Fig. 5 Experimental curves of load–displacement for the six specimens in the same batch

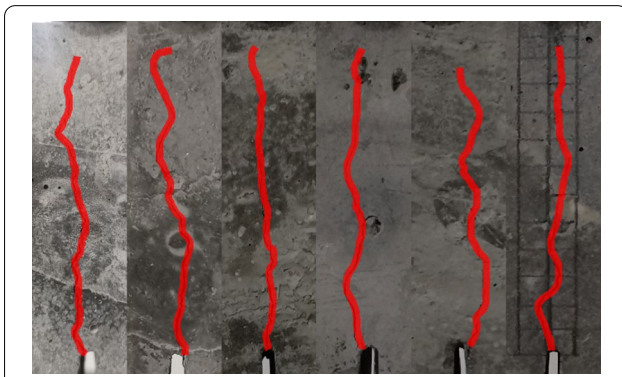


Fig. 6 Experimental crack propagation paths for the six specimens in the same batch

The load–displacement curves of the fracture process and the crack propagation paths were recorded, as shown in Figs. 5 and 6. Due to inhomogeneity and randomness

Table 3 Total area of packed coarse aggregates with different particle sizes

Particle size range (mm)	Real aggregate area (mm ²)	Circular aggregate area (mm ²)
4.75–9.5	6191.99	6877.55
9.5–16.0	7780.10	8641.50
16.0–19.0	2407.07	2673.58
19.0–26.5	1353.86	1503.76

of the internal structure of concrete, the load–displacement curves are highly dispersed, but they all have obvious three stages, namely, rising stage, sharp falling stage and gentle falling stage. The average peak fracture load is about 6.545 kN. The crack paths are highlighted in red in Fig. 6 for easy observation. It can be seen that, although the crack paths are very tortuous and have significant differences, they all have a tendency to go straight forward. They originate from the tip of the notch, and put their end points near the loading head.

2.4 Validation of Numerical Modeling Method

According to Table 1, after excluding fine aggregates with particle sizes less than 4.75 mm, the total areas of packed coarse aggregates with different particle sizes were calculated, as shown in Table 3. Then, the parameterization modeling (Yang et al., 2012; Yin et al., 2011, 2012, 2015) was adopted to randomly pack 253 aggregates with different particle sizes into a rectangular area with a length of 400 mm and a width of 100 mm. After the geometric modeling was completed, a two-dimensional three-point bending concrete beam model was obtained and then a 20 mm deep notch located in the middle of its bottom, as shown in Fig. 7.

The geometric model was discretized with the triangular plane stress solid elements and two-dimensional 0-thickness cohesive elements. Fig. 8 exhibits the finite-element mesh with the highlighted cohesive elements in the mortar for (a) and in the ITZ for (b), respectively. The efficiency and accuracy of numerical simulation depend on the finite-element grid density (Zhang et al., 2018b). In general, the denser the grid is, the more accurate the calculation is, but the higher the time cost of the calculation is. To seek a balance between the accuracy and efficiency of the calculation, the element size was changed from 0.75 to 1.00 mm, 1.50 mm, and 2.00 mm. It was proved that the mesh size of 1.50 mm could balance the efficiency and accuracy. In this case, the computational model totally has 75,447 nodes, 37,779 solid elements, 29,704 mortar matrix cohesive elements and 4664 ITZ cohesive elements.

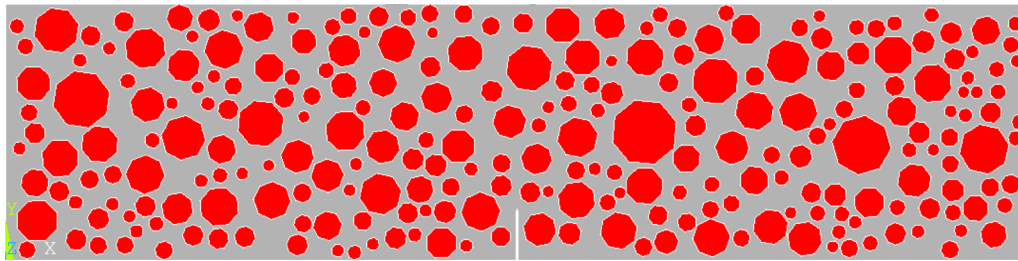
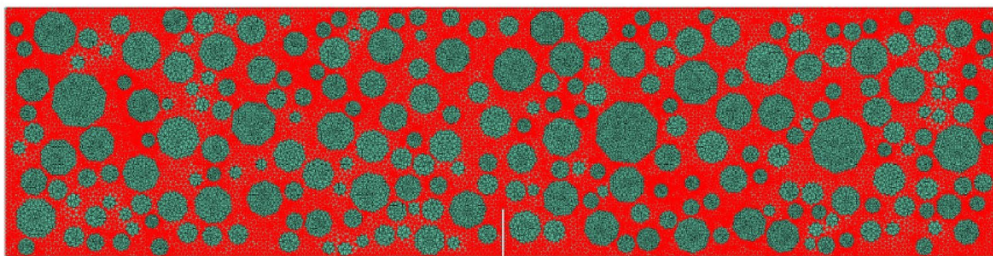
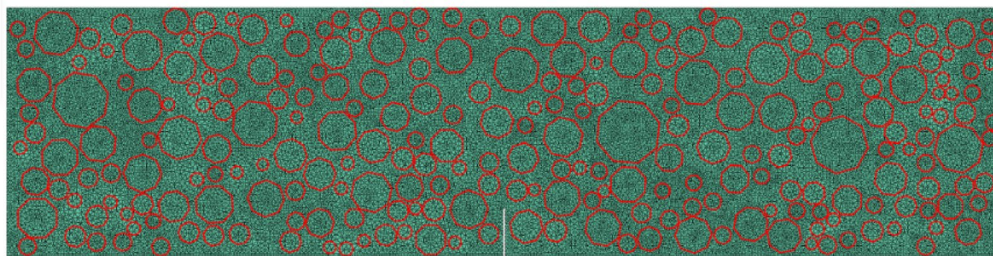


Fig. 7 Geometric model of concrete three-point bending beam



(a) Highlighted cohesive elements in the mortar



(b) Highlighted cohesive elements in the ITZ

Fig. 8 Finite-element grid model of concrete three-point bending beam with the cohesive elements

Table 4 Material parameters

Components	<i>E</i> (GPa)	ν	t_0 (MPa)	<i>G</i> (N/m)
Aggregate	40	0.2	–	–
Mortar	20	0.2	3.058	158.1
ITZ	–	–	2.508	147.6

The solid elements and cohesive elements were characterized with the linear elastic model and bilinear softening model, respectively. Their material parameters are shown in Table 4 (Ji et al., 2020; Zhang et al., 2016, 2018a, 2018b; Zou et al., 2021). The tensile strengths and fracture energies of mortar and ITZ were obtained through the splitting tensile test (Zou et al., 2021) and

three-point bending test on the granite-mortar hybrid specimens and pure mortar specimens (Ji et al., 2020). The tangential parameters of the cohesive elements were assumed to be the same as the corresponding normal parameters (Zhang et al., 2016, 2018a, 2018b). The loads and constraints are shown in Fig. 9. A displacement load from 0 to 0.6 mm was applied. It includes 10,000 load steps with a constant load increment.

Fig. 10 shows the load–displacement curve. For comparison, the envelope region of the experimental load–displacement curves for the six specimens in the same batch is also given in this figure. It can be seen that the numerical load–displacement curve completely fall within the experimental envelope region. The numerical peak load is 5.688 kN, which is about

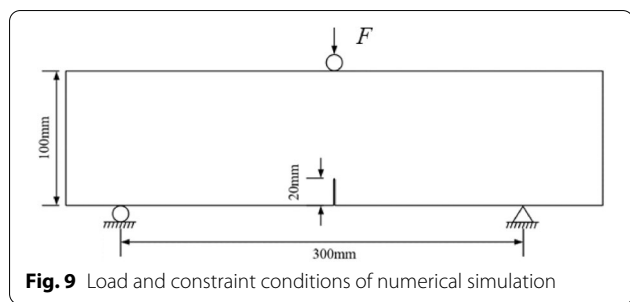


Fig. 9 Load and constraint conditions of numerical simulation

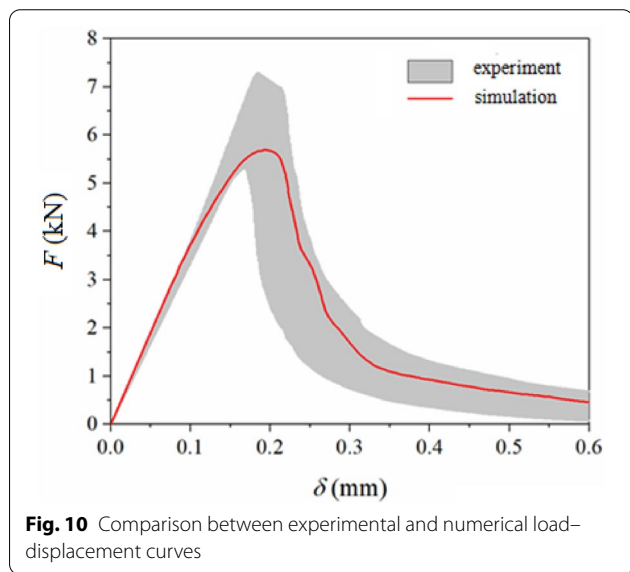


Fig. 10 Comparison between experimental and numerical load–displacement curves

13.09% lower than the experimental average peak load of 6.545 kN. Considering the following factors, this difference is acceptable: (1) the size, shape and position of the aggregates inside the concrete are random, and the constitutive model parameters of different component materials are approximate, so the numerical model cannot be completely consistent with the physical truth; (2) There are certain errors in the constraint and loading locations, specimen and notch geometries, and so on; (3) A two-dimensional model with the plane stress assumption is used for the numerical simulation; (4) In the process of making and cutting concrete specimens, it is inevitable to introduce initial defects and damage. Fig. 11 shows the experimental and numerical crack propagation paths. As you can see, they have a very good consistency in shape and trend. This indicates that all the used numerical simulation method, constitutive models and their parameters are reasonable.

It should be pointed out that coarse aggregate distribution generally has very slight effect on the pre-peak mechanical behaviors but significant effect on the post-peak behavior. Considering that the aggregate

distribution effect was carefully evaluated (Yin et al., 2012; Zhang et al., 2016), it is no longer discussed here.

3 Results and Analyses

In this section, the numerical simulation method was adopted to study the effects of the water–cement ratio of mortar, the roughness of bonding surface and the content of silica fume in interface agent on the tensile fracture properties of concrete.

3.1 Computational Model and Conditions

The parameterization modeling (Yang et al., 2012; Yin et al., 2011, 2012, 2015) was used to establish a two-dimensional concrete model with the size of 100 mm × 100 mm. In the model, coarse aggregate has the total area content of 44.33%, so the packed circular aggregate has the total area content of 49.24%. According to Table 1, the areas of coarse aggregates with different particle sizes were calculated, as shown in Table 5. In the numerical simulation, the material parameters of ITZ and mortar were changed according to the varying mortar water–cement ratio, bonding surface roughness and silica fume content in the interface agent, while the other material parameters remained unchanged. The lateral and longitudinal displacements of the lower surface of the model were constrained, and the upper surface was subjected to a longitudinal displacement increasing from 0 to 0.16 mm at a constant rate of 1.6 mm/s, as shown in Fig. 12. A series of tensile fracture simulations were carried out.

3.2 Effect of Mortar Water–Cement Ratio

The water–cement ratio of mortar is an important factor affecting the mechanical properties of concrete. Increasing the water–cement ratio would increase the porosity of ITZ and weaken the aggregate–mortar bonding. The splitting tensile test on the granite–mortar hybrid specimens (Zou et al., 2021) showed that the tensile strength of ITZ is relative to the water–cement ratio of mortar by

$$f_{st} = -9.296w/c + 5.872 \tag{1}$$

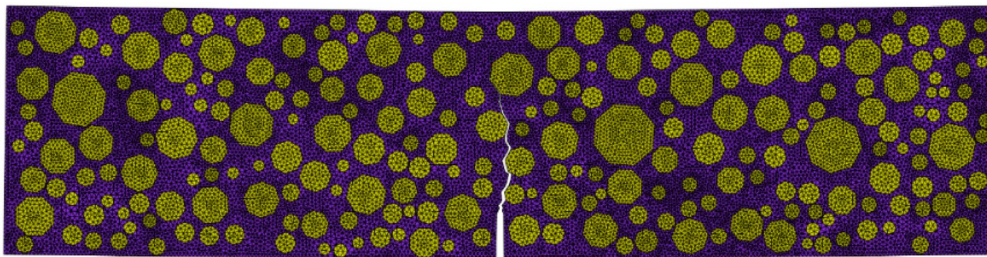
The unit of the tensile strength is MPa. From the splitting tensile test on the pure mortar specimens, the tensile strength of mortar experimentally depends on the water–cement ratio of mortar by Zou et al. (2021)

$$f_{st} = -5.427w/c + 5.730 \tag{2}$$

On the other hand, according to the three-point bending test on the granite-mortar hybrid beams, there is the following connection between the ITZ fracture energy and the mortar water–cement ratio (Ji et al., 2020).



(a) Experimental crack propagation path



(b) Numerical crack propagation path

Fig. 11 Comparison between experimental and numerical crack propagation paths

Table 5 Packed coarse aggregate areas at all levels of particle size

Particle size range (mm)	Real aggregate area (mm ²)	Round aggregate area (mm ²)
4.75–9.5	1547.99	1719.39
9.5–16.0	1945.03	2160.38
16.0–19.0	601.76	668.39
19.0–26.5	338.46	375.94

$$G = -167.448w/c + 124.468 \tag{3}$$

The unit of the fracture energy is N/m. From the three-point bending test on the pure mortar beams, the mortar fracture energy is expressed in terms of the mortar water–cement ratio as (Ji et al., 2020)

$$G = -564.540w/c + 433.978 \tag{4}$$

Considering that the water–cement ratio of mortar has a range from 0.3 to 0.5 in the three-point bending test and splitting tensile test, the tensile fracture behaviors of concrete were investigated when the water–cement ratio of mortar was 0.3, 0.35, 0.4, 0.45 and 0.5, respectively. Fig. 13 shows the load–displacement curves for different mortar water–cement ratios. It can be seen that with the decrease of mortar water–cement ratio, both the peak

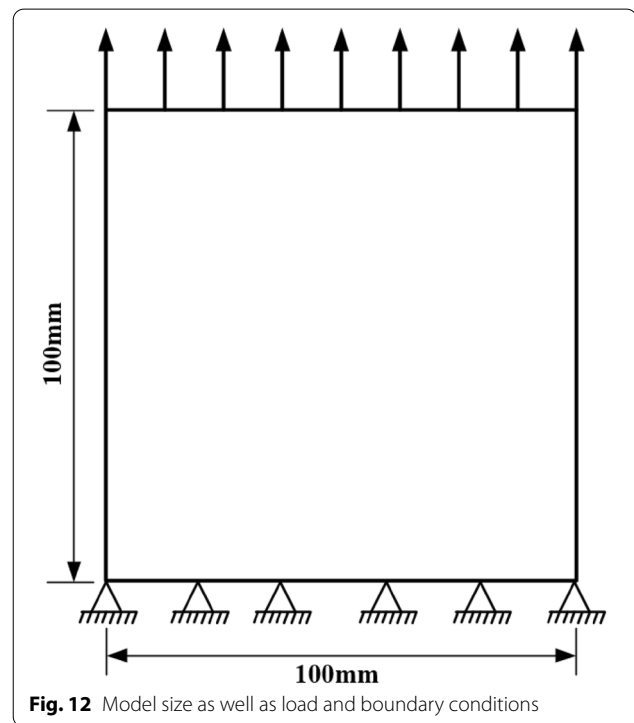
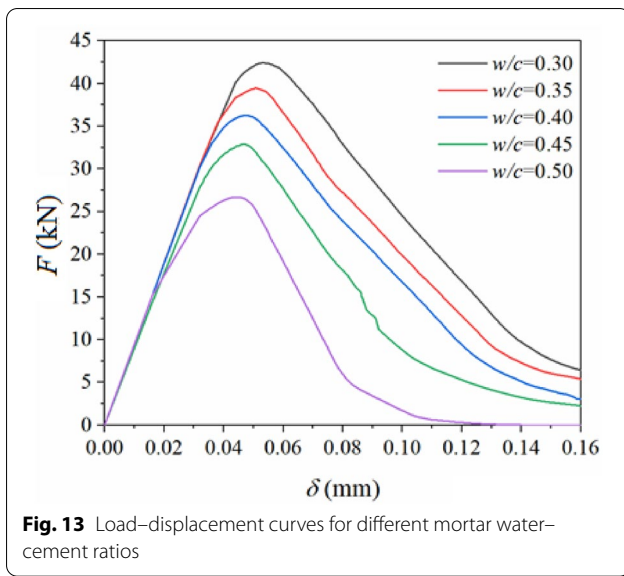


Fig. 12 Model size as well as load and boundary conditions

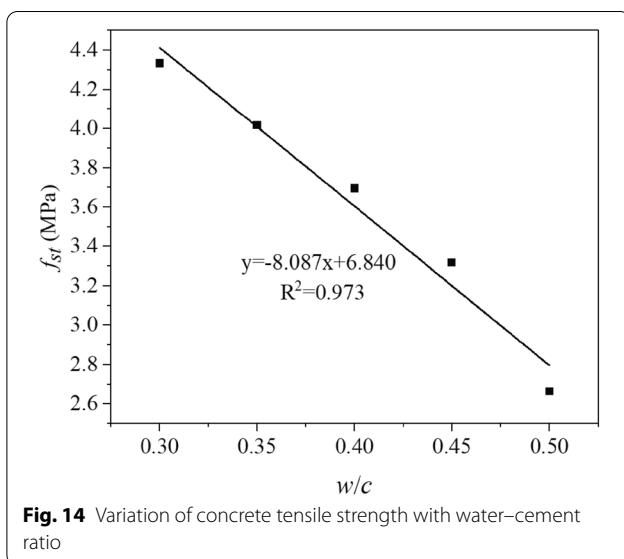
load and dissipated fracture energy increase significantly. With the mortar water–cement ratio decreasing from 0.5 to 0.45, 0.4, 0.35 and 0.3, the peak load increases by



24.6%, 38.8%, 50.9% and 62.8%, respectively. The influence of water–cement ratio on the post-peak deflection behavior of concrete does not seem consistent with common perception that a lower water–cement ratio generally leads to more brittle concrete. However, it is also noticed from Fig. 13 that this influence is mainly from the impact of water–cement ratio on the peak load. Therefore, the above inconsistency is easy to understand.

$$f_{st} = -8.087w/c + 6.840 \tag{5}$$

Fig. 14 shows the variation of tensile strength of concrete with the water–cement ratio of mortar. The



relationship between them can be established by linear regression analysis as follows.

Fig. 15 shows the variation of the dissipated energy of concrete in the process of tensile fracture with the mortar water–cement ratio. The relationship between them can also be established by linear regression analysis as follows.

$$W = -9.402w/c + 6.390 \tag{6}$$

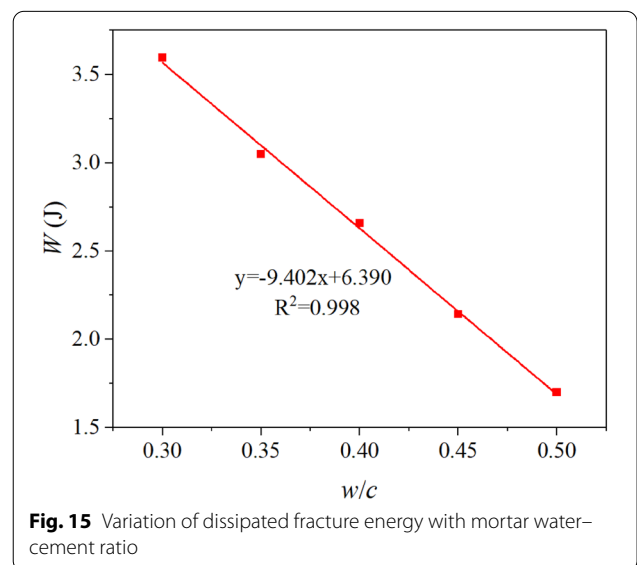
3.3 Effect of Aggregate Surface Roughness

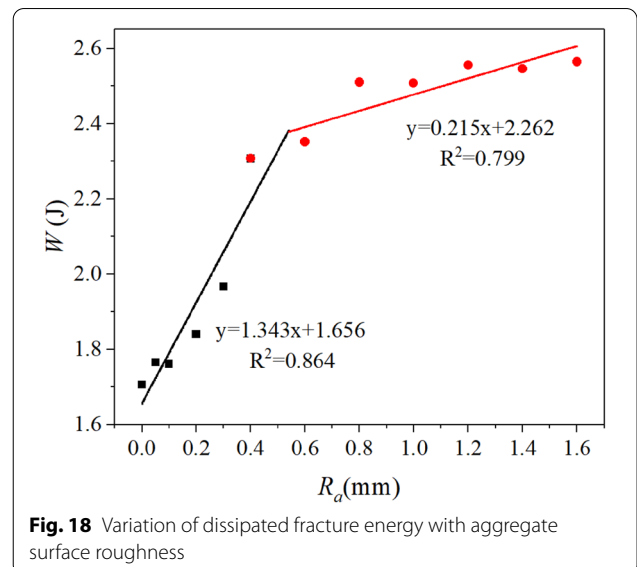
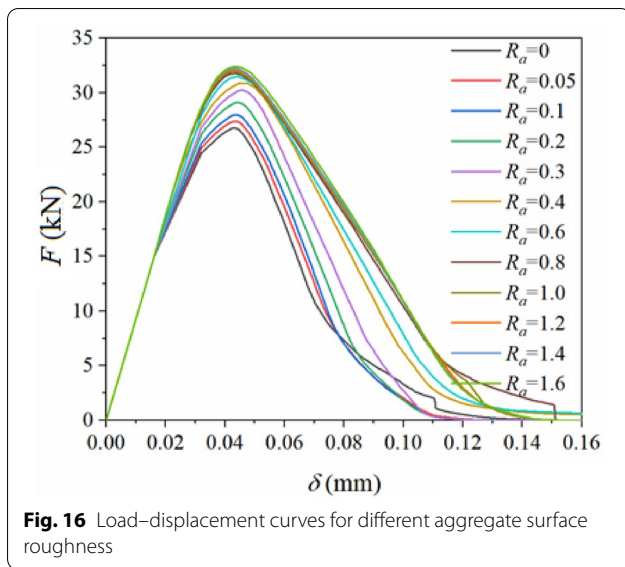
The aggregate surface roughness significantly affects the interfacial strength (Guinea et al., 2002; Santos & Júlio, 2013). The experimental studies (Ji et al., 2020; Rao & Prasad, 2004) showed that the increase of aggregate surface roughness can significantly improve the tensile strength and fracture energy of ITZ. According to the splitting tensile test on the granite-mortar hybrid specimens (Zou et al., 2021) and the three-point bending test on the granite-mortar hybrid beams (Ji et al., 2020), the tensile strength and fracture energy of ITZ have the following connections with the aggregate surface roughness (Ji et al., 2020; Zou et al., 2021).

$$f_{st} = 0.849R_a + 1.234 \tag{7}$$

$$G = 73.696R_a + 37.094 \tag{8}$$

The tensile fracture behaviors of concrete were simulated for different cases of the aggregate surface roughness. Fig. 16 shows the load–displacement curves for different aggregate surface roughness. It can be seen that the peak load of concrete increases with the increase of





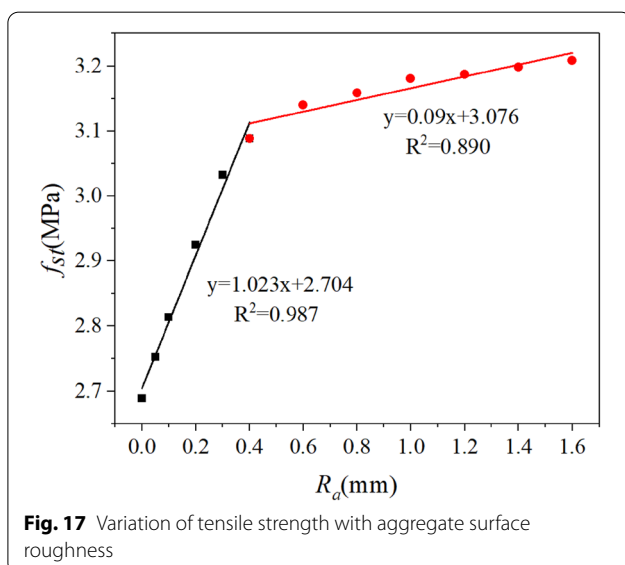
aggregate surface roughness, and the load–displacement curves start to separate before the load reaches its peak value. With the increase of displacement, their gap becomes more and more prominent. This is mainly because the interface bonding strength increases with the increase of aggregate surface roughness. The higher the bonding strength of the interface is, the greater the energy required for fracture is. As a result, the area enclosed by the load–displacement curve and the horizontal axis is also larger.

Figs. 17 and 18, respectively, show the variations of the tensile strength and the dissipated energy with the aggregate surface roughness. Hong et al. (2014) also studied

the influence of coarse aggregate surface roughness on the tensile properties of concrete through experiments. Compared to their results, the curves are consistent in shape and trend. Through linear regression analysis, the relations of the tensile strength and dissipated energy of concrete with the surface roughness of coarse aggregate can be established as follows.

$$f_{st} = \begin{cases} 1.023R_a + 2.704 & 0 \leq R_a \leq 0.4 \\ 0.09R_a + 3.076 & 0.4 < R_a \leq 1.6 \end{cases} \quad (9)$$

$$W = \begin{cases} 1.343R_a + 2.656 & 0 \leq R_a \leq 0.4 \\ 0.215R_a + 2.262 & 0.4 < R_a \leq 1.6 \end{cases} \quad (10)$$



Generally speaking, the effects of aggregate surface roughness on the tensile fracture properties of concrete are very complicated. For the aggregate surface roughness between 0 and 0.4 mm, both the tensile strength and dissipated energy of concrete increase rapidly with increasing aggregate surface roughness. This is because when the aggregate surface roughness is small, the mechanical properties of ITZ are much weaker than those of mortar. With the increase of aggregate surface roughness, the mechanical properties of ITZ gradually approach those of mortar, so that the proportion of exposed aggregate area in the fracture surface decreases gradually. Fig. 19a–c, respectively, shows the tensile fracture paths of aggregate surface roughness of 0, 0.2 mm and 0.4 mm.

For the aggregate surface roughness from 0.6 to 1.6 mm, with the increase of aggregate surface

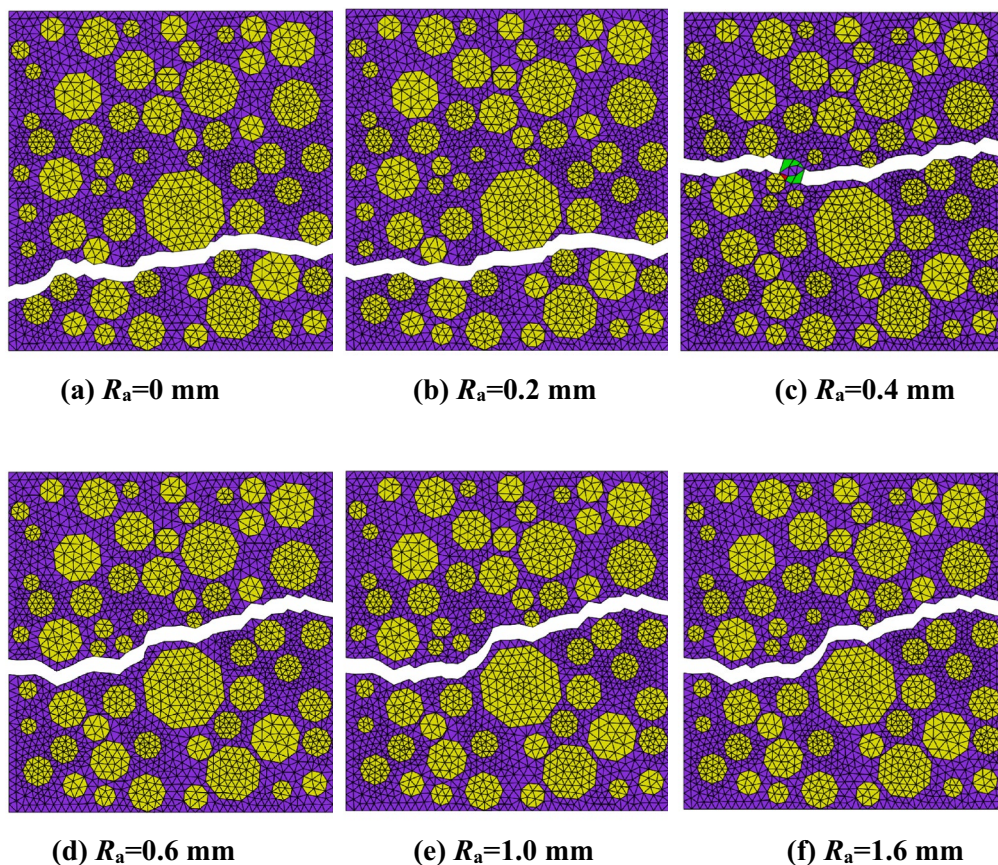


Fig. 19 Tensile fracture paths for different aggregate roughness

roughness, the tensile strength and dissipated energy of concrete still increase, but very slowly. This is because the mechanical properties of ITZ are almost the same as those of mortar. Fig. 19d–f, respectively, shows the tensile fracture paths for aggregate surface roughness of 0.6 mm, 1 mm and 1.6 mm. It can be seen that the exposed aggregates at the fracture appearance is very few, and the area of the exposed aggregates changes very little when the aggregate surface roughness continues to increase. Therefore, the mechanical properties of concrete are no longer sensitive to the change of aggregate surface roughness.

Hong et al. (2014) carried out the tensile fracture experiments on the spherical high boric acid aggregate concrete with different roughness, and found that the exposed aggregate area at the fracture appearance for the smooth aggregate concrete is larger and the tensile strength was lower than that for striated aggregate concrete aggregate with surface incision treatment. This is consistent with the above results.

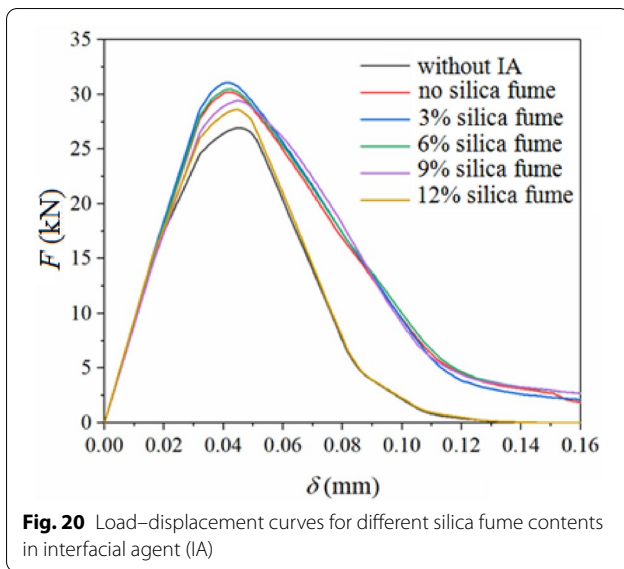
3.4 Effect of Silica Fume Content in Interfacial Agent

Due to the pozzolanic ash effect and micro-aggregate effect (Abu Noaman et al., 2019; Sankar et al., 2020), a layer of interfacial agent containing silica fume on aggregate surface can effectively reduce the porosity of ITZ and improve its mechanical properties. The experimental results from the splitting tensile test on the granite-mortar hybrid specimens (Zou et al., 2021) and the three-point bending test on the granite-mortar hybrid beams (Ji et al., 2020) showed that the tensile strength and fracture energy of ITZ have the following connections with the silica fume content in interfacial agent.

$$f_{st} = -0.005f^2 + 0.031f + 1.706 \tag{11}$$

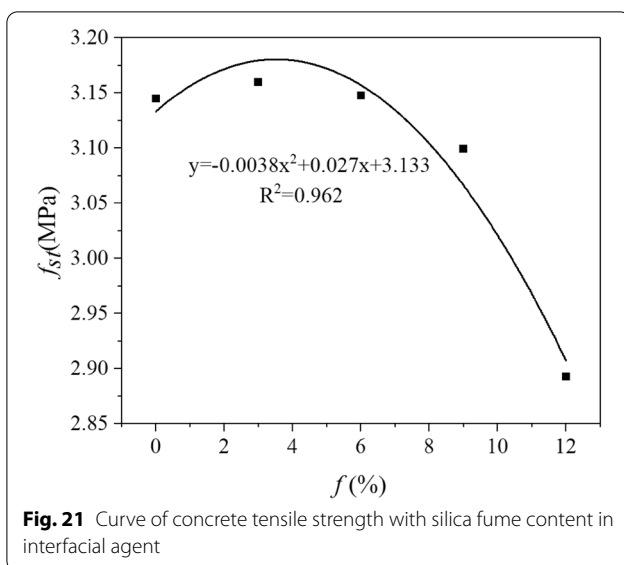
$$G = -0.2063f^2 + 1.987f + 53.853 \tag{12}$$

Fig. 20 shows the load–displacement curves for different silica fume contents in interfacial agent wrapped on the aggregate surface. It can be seen that, compared



with the case without interfacial agent on aggregate surface, the peak loads of concrete for the cases with interfacial agent containing 0, 3%, 6%, 9% and 12% silica fume increase by 15.2%, 15.8%, 15.3%, 13.5% and 6.0%, respectively. When the content of silica fume is about 3%, the peak load is the highest.

Fig. 21 shows the variation of the tensile strength of concrete with the silica fume content in the interface agent. It can be seen that the effect of silica fume content on the tensile strength of concrete is complex. When the silica fume content is between 0 and 3%, the tensile strength of concrete increases slightly with the increase of silica fume content, but when the silica fume



content is between 3% and 12%, the tensile strength of concrete decreases significantly with the increase of silica fume content. This is qualitatively consistent with the experimental results of high performance concrete (HPC) (Ji et al., 2020). Smarzewski (Ji et al., 2020) found that the tensile strength of HPC increases with growing silica fume content up to 10%, but reduces with the further increase of silica fume content from 10% to 25%, and fitted their relationship with a quadratic parabolic curve. In addition, it is noticed that, different from the additive of silica fume to interface agent in this study, Smarzewski added silica fume to cement paste in his experiments.

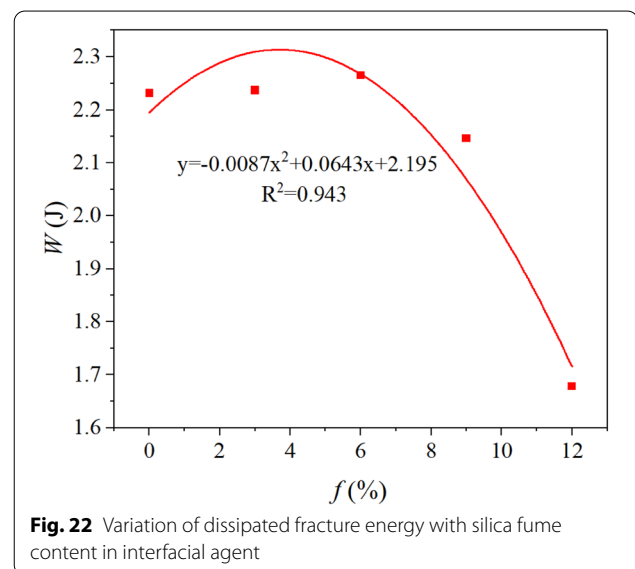
Similarly, the relationship between the tensile strength of concrete and silica fume content in interfacial agent can be fitted by the following quadratic parabolic function.

$$f_{st} = -0.0038f^2 + 0.027f + 3.133 \quad (13)$$

Fig. 22 shows the variation of the dissipated energy of concrete complete fracture with the content of silica fume in interfacial agent. It can be seen that the variation of the dissipated energy varies is very similar to the variation of tensile strength with the content of silica fume in interfacial agent. Their relationship can also be fitted by a quadratic parabolic function.

$$W = -0.0087f^2 + 0.0643f + 2.195 \quad (14)$$

According to Eqs. (13) and (14), the tensile fracture mechanical properties of concrete have an approximate quadratic parabola relationship with the content



of silica fume in the interfacial agent, and the optimal content of silica fume is roughly between 3.5% and 3.7%.

4 Conclusions

The parameterization modeling was used to establish the model of heterogeneous concrete with aggregate size and distribution information and the bilinear cohesive zone constitutive model was used to describe the cracking behavior of mortar and ITZ. Through mediating the mechanical properties of ITZ based on the experiments, the influences of the water–cement ratio of mortar, the surface roughness of coarse aggregate and the content of silica fume in interfacial agent on the tensile fracture behavior of concrete were quantitatively studied by the numerical simulation. The following conclusions were drawn.

- (1) The tensile fracture properties of concrete are closely related to the water–cement ratio of mortar. With the decrease of water–cement ratio of mortar, both the tensile strength and dissipated fracture energy of concrete increase significantly. They have a negative linear correlation with the water–cement ratio of mortar.
- (2) The surface roughness of coarse aggregate has a great influence on the tensile fracture properties of concrete, and both the tensile strength and dissipated fracture energy have a bilinear relationship with the surface roughness of coarse aggregate. When the aggregate surface roughness increases from 0 to 0.4 mm, both the tensile strength and dissipated energy of concrete increase rapidly. When the aggregate surface roughness increases from 0.6 to 1.6 mm, however, the tensile strength and dissipated energy of concrete increase very slowly.
- (3) The tensile strength and dissipated fracture energy of concrete have an approximate quadratic parabola relationship with the content of silica fume in the interfacial agent. The best tensile fracture properties of concrete can be obtained by wrapping a layer of interfacial agent with a content of 3.5–3.7% of silica fume on the aggregate surface.

In addition, it must be pointed that the validity of the above results and conclusions should be limited within the discussed scopes of the water–cement ratio of mortar, the surface roughness of coarse aggregate and the content of silica fume in interfacial agent in this paper.

Acknowledgements

Not applicable.

Author contributions

The first author, HJ conducted the experiments, data analyses and numerical simulations. The corresponding author, XY supervised the project, completed the model, and wrote the manuscript. The third author, ZL participated in the experiments and data analysis. The fourth author, FB participated in the numerical simulations. All authors read and approved the final manuscript.

Authors' information

Heli Ji, Master Student, School of Aerospace Engineering, Huazhong University of Science and Technology, Wuhan 430074, China. Xinhua Yang, Distinguished Professor, School of Transportation, Civil Engineering and Architecture, Foshan University, Foshan 528200, China, and Professor, School of Aerospace Engineering, Huazhong University of Science and Technology. Zuyun Luo: Master Student, School of Aerospace Engineering, Huazhong University of Science and Technology, Wuhan 430074, China. Fan Bai, Associate Professor, College of Science, Wuhan University of Science and Technology, Wuhan 430065, China.

Funding

This work was supported by the National Natural Science Foundation of China (Grant Nos 11832013 and 12072120).

Availability of data and materials

The data sets used and/or analyzed during the current study are available from the corresponding author on reasonable request.

Declarations

Competing interests

The authors declare that they have no competing interests.

Author details

¹School of Transportation, Civil Engineering and Architecture, Foshan University, Foshan 528200, China. ²School of Aerospace Engineering, Huazhong University of Science and Technology, Wuhan 430074, China. ³College of Science, Wuhan University of Science and Technology, Wuhan 430065, China.

Received: 2 June 2022 Accepted: 28 September 2022

Published online: 10 January 2023

References

- Abu Noaman, M., Karim, M. R., & Islam, M. N. (2019). Comparative study of pozzolanic and filler effect of rice husk ash on the mechanical properties and microstructure of brick aggregate concrete. *Heliyon*, *5*, e1926.
- Asbridge, A. H., Chadborn, G. A., & Page, C. L. (2001). Effects of metakaolin and the interfacial transition zone on the diffusion of chloride ions through cement mortars. *Cement and Concrete Research*, *31*, 1567–1572.
- Bourdette, B., Ringot, E., & Ollivier, J. P. (1995). Modelling of the transition zone porosity. *Cement and Concrete Research*, *25*, 741–751.
- Brand, A. S., & Roesler, J. R. (2017a). Bonding in cementitious materials with asphalt-coated particles: Part I—The interfacial transition zone. *Construction and Building Materials*, *130*, 171–181.
- Brand, A. S., & Roesler, J. R. (2017b). Bonding in cementitious materials with asphalt-coated particles: Part II—Cement–asphalt chemical interactions. *Construction and Building Materials*, *130*, 182–192.
- Bui, D. D., Hu, J., & Stroeven, P. (2005). Particle size effect on the strength of rice husk ash blended gap-graded Portland cement concrete. *Cement and Concrete Composites*, *27*, 357–366.
- Caliskan, S. (2003). Aggregate/mortar interface: Influence of silica fume at the micro- and macro-level. *Cement and Concrete Composites*, *25*, 557–564.
- Chen, J., & Qian, C. (2017). Loading history dependence of retardation time of calcium-silicate-hydrate. *Construction and Building Materials*, *147*, 558–565.
- Ding, H., & Chen, J. (2019). Research on the resistivity attenuation law of cementitious conductive composites induced by stress relaxation. *Construction and Building Materials*, *206*, 347–354.

- Duan, P., Shui, Z., Chen, W., & Shen, C. (2013). Effects of metakaolin, silica fume and slag on pore structure, interfacial transition zone and compressive strength of concrete. *Construction and Building Materials*, *44*, 1–6.
- Golewski, G. L. (2021a). The beneficial effect of the addition of fly ash on reduction of the size of microcracks in the ITZ of concrete composites under dynamic loading. *Energies*, *14*, 668.
- Golewski, G. L. (2021b). Validation of the favorable quantity of fly ash in concrete and analysis of crack propagation and its length—Using the crack tip tracking (CTT) method—In the fracture toughness examinations under Mode II, through digital image correlation. *Construction and Building Materials*, *296*, 122362.
- Golewski, G. L. (2021c). Evaluation of fracture processes under shear with the use of DIC technique in fly ash concrete and accurate measurement of crack path lengths with the use of a new crack tip tracking method. *Measurement*, *181*, 109632.
- Gu, X., Hong, L., Wang, Z., & Lin, F. (2013). Experimental study and application of mechanical properties for the interface between cobblestone aggregate and mortar in concrete. *Construction and Building Materials*, *46*, 156–166.
- Guinea, G. V., El-Sayed, K., Rocco, C. G., Elices, M., & Planas, J. (2002). The effect of the bond between the matrix and the aggregates on the cracking mechanism and fracture parameters of concrete. *Cement and Concrete Research*, *32*, 1961–1970.
- Hong, L., Gu, X., & Lin, F. (2014). Influence of aggregate surface roughness on mechanical properties of interface and concrete. *Construction and Building Materials*, *65*, 338–349.
- Ji, H., Yang, X., & Luo, Z. (2020). Experimental study of fracture properties of interfacial transition zone by three-point bending tests on granite–mortar hybrid beams. *Construction and Building Materials*, *263*, 120605.
- Jiang, L. (1999). The interfacial zone and bond strength between aggregates and cement pastes incorporating high volumes of fly ash. *Cement and Concrete Composites*, *21*, 313–316.
- Kuroda, M., Watanabe, T., & Terashi, N. (2000). Increase of bond strength at interfacial transition zone by the use of fly ash. *Cement and Concrete Research*, *30*, 253–258.
- Li, Y., & Metcalf, J. B. (2005). Two-step approach to prediction of asphalt concrete modulus from two-phase micromechanical models. *Journal of Materials in Civil Engineering*, *17*, 407–415.
- Liao, K., Chang, P., Peng, Y., & Yang, C. (2004). A study on characteristics of interfacial transition zone in concrete. *Cement and Concrete Research*, *34*, 977–989.
- Manzoli, O. L., Maedo, M. A., Bitencourt, L. A. G., Jr., & Rodrigues, E. A. (2016). On the use of finite elements with a high aspect ratio for modeling cracks in quasi-brittle materials. *Engineering Fracture Mechanics*, *153*, 151–170.
- Rao, G. A., & Prasad, B. K. R. (2004). Influence of type of aggregate and surface roughness on the interface fracture properties. *Materials and Structures*, *37*, 328–334.
- Rodrigues, E. A., Gimenes, M., Bitencourt, L. A. G., Jr., & Manzoli, O. L. (2021). A concurrent multiscale approach for modeling recycled aggregate concrete. *Construction and Building Materials*, *267*, 121040.
- Rodriguesa, E. A., Manzolia, O. L., & Bitencourt, L. A. G. (2020). 3D concurrent multiscale model for crack propagation in concrete. *Computer Methods in Applied Mechanics and Engineering*, *361*, 112813.
- Rossignolo, J. A. (2009). Interfacial interactions in concretes with silica fume and SBR latex. *Construction and Building Materials*, *23*, 817–821.
- Sánchez, M., Manzoli, O. L., & Guimarães, L. (2014). Modeling 3-D desiccation soil crack networks using a mesh fragmentation technique. *Computers and Geotechnics*, *62*, 27–39.
- Sankar, L. P., Sivasankar, S., Shunmugasundaram, M., & Praveen Kumar, A. (2020). Investigation on binder and concrete with fine grinded fly ash and silica fume as pozzolanic combined replacement. *Materials Today Proceedings*, *27*, 1157–1162.
- Santos, P. M. D., & Júlio, E. N. B. S. (2013). A state-of-the-art review on roughness quantification methods for concrete surfaces. *Construction and Building Materials*, *38*, 912–923.
- Scrivener, K. L., Crumie, A. K., & Laugesen, P. (2004). The interfacial transition zone (ITZ) between cement paste and aggregate in concrete. *Interface Science*, *12*, 411–421.
- Shen, Y., Wang, Y., Yang, Y., Sun, Q., Luo, T., & Zhang, H. (2019). Influence of surface roughness and hydrophilicity on bonding strength of concrete–rock interface. *Construction and Building Materials*, *213*, 156–166.
- Siddique, R. (2011). Utilization of silica fume in concrete: Review of hardened properties. *Resources, Conservation and Recycling*, *55*, 923–932.
- Smarzewski, P. (2019). Influence of silica fume on mechanical and fracture properties of high performance concrete. *Procedia Structural Integrity*, *17*, 5–12.
- Szostak, B., & Golewski, G. L. (2020). Improvement of strength parameters of cement matrix with the addition of siliceous fly ash by using nanometric C–S–H seeds. *Energies*, *13*, 6734.
- Tschegg, E. K., Rotter, H. M., Roelfstra, P. E., Bourkund, U., & Jussel, P. (1995). Fracture mechanical behavior of aggregate–cement matrix interfaces. *Journal of Materials in Civil Engineering*, *7*, 199–203.
- Wu, K., Shi, H., Xu, L., Ye, G., & De Schutter, G. (2016). Microstructural characterization of ITZ in blended cement concretes and its relation to transport properties. *Cement and Concrete Research*, *79*, 243–256.
- Yang, C. C. (1998). Effect of the transition zone on the elastic moduli of mortar. *Cement and Concrete Research*, *28*, 727–736.
- Yang, S. F., Yang, X. H., Yin, A. Y., & Jiang, W. (2012). Three-dimensional numerical evaluation of influence factors of mechanical properties of asphalt mixture. *Journal of Mechanics*, *28*, 569–578.
- Yin, A., Yang, X., Gao, H., & Zhu, H. (2012). Tensile fracture simulation of random heterogeneous asphalt mixture with cohesive crack model. *Engineering Fracture Mechanics*, *92*, 40–55.
- Yin, A., Yang, X., Yang, S., & Jiang, W. (2011). Multiscale fracture simulation of three-point bending asphalt mixture beam considering material heterogeneity. *Engineering Fracture Mechanics*, *78*, 2414–2428.
- Yin, A., Yang, X., Zhang, C., Zeng, G., & Yang, Z. (2015). Three-dimensional heterogeneous fracture simulation of asphalt mixture under uniaxial tension with cohesive crack model. *Construction and Building Materials*, *76*, 103–117.
- Zhang, P., & Li, Q. F. (2012). Effect of silica fume on fracture properties of high-performance concrete containing fly ash. *Journal of Materials: Design and Applications*, *227*, 336–342.
- Zhang, C., Yang, X., & Gao, H. (2018a). Effect of randomness of interfacial properties on fracture behavior of concrete under uniaxial tension. *Acta Mechanica Solida Sinica*, *31*, 174–186.
- Zhang, C., Yang, X., & Gao, H. (2018b). Air-void-affected zone in concrete beam under four-point bending fracture. *Journal of Civil Engineering and Management*, *24*, 130–137.
- Zhang, C., Yang, X., Gao, H., & Zhu, H. (2016). Heterogeneous fracture simulation of three-point bending plain-concrete beam with double notches. *Acta Mechanica Solida Sinica*, *29*, 232–244.
- Zheng, Z., Wei, X., & Tian, C. (2021). Mesoscale models and uniaxial tensile numerical simulations of concrete considering material heterogeneity and spatial correlation. *Construction and Building Materials*, *312*, 125428.
- Zou, X., Ji, H., Yang, X., Luo, Z., & Bai, F. (2021). Experimental study of fracture property of granite–mortar interfacial transition zone. *Journal of Civil Engineering and Management*, *38*(6), 17–24. [https://doi.org/10.13579/j.cnki.2095-0985.2021.06.003\(InChinese\)](https://doi.org/10.13579/j.cnki.2095-0985.2021.06.003(InChinese))

Publisher's Note

Springer Nature remains neutral with regard to jurisdictional claims in published maps and institutional affiliations.